

Geophysical Research Letters[®]



RESEARCH LETTER

10.1029/2023GL102816

Key Points:

- Minimal snow was lost into leads in observations of three cases in typical wintertime, cold, moderately windy conditions on Arctic sea ice
- In an atmospheric advection event with air temperature above -10°C , high wind, and fresh snowfall, most recent snowfall was lost into leads
- Warm air temperatures increase the duration of unfrozen water in leads, which may be an underappreciated factor in snow loss into leads

Supporting Information:

Supporting Information may be found in the online version of this article.

Correspondence to:

D. Clemens-Sewall,
dcsewall@ucar.edu













Citation:

Clemens-Sewall, D., Polashenski, C., Frey, M. M., Cox, C. J., Granskog, M. A., Macfarlane, A. R., et al. (2023). Snow loss into leads in Arctic sea ice: Minimal in typical wintertime conditions, but high during a warm and windy snowfall event. *Geophysical Research Letters*, 50, e2023GL102816. <https://doi.org/10.1029/2023GL102816>

Received 4 FEB 2023

Accepted 5 JUN 2023

Snow Loss Into Leads in Arctic Sea Ice: Minimal in Typical Wintertime Conditions, but High During a Warm and Windy Snowfall Event

David Clemens-Sewall¹ , Chris Polashenski^{1,2} , Markus M. Frey³ , Christopher J. Cox⁴ , Mats A. Granskog⁵ , Amy R. Macfarlane⁶ , Steven W. Fons^{7,8} , Julia Schmale⁹ , Jennifer K. Hutchings¹⁰ , Luisa von Albedyll¹¹ , Stefanie Arndt¹¹ , Martin Schneebeli⁶ , and Don Perovich¹ 

¹Thayer School of Engineering, Dartmouth College, Hanover, NH, USA, ²Cold Regions Research and Engineering Laboratory, US Army Corps of Engineers, Hanover, NH, USA, ³British Antarctic Survey—Natural Environment Research Council, Cambridge, UK, ⁴NOAA Physical Sciences Laboratory, Boulder, CO, USA, ⁵Fram Centre, Norwegian Polar Institute, Tromsø, Norway, ⁶WSL Institute for Snow and Avalanche Research SLF, Davos, Switzerland, ⁷Cryospheric Sciences Laboratory, NASA Goddard Space Flight Center, Greenbelt, MD, USA, ⁸Earth System Science Interdisciplinary Center, University of Maryland, College Park, MD, USA, ⁹Extreme Environments Research Laboratory, École Polytechnique Fédérale de Lausanne, Sion, Switzerland, ¹⁰College of Earth, Ocean, and Atmospheric Sciences, Oregon State University, Corvallis, OR, USA, ¹¹Alfred-Wegener-Institut, Helmholtz-Zentrum für Polar- und Meeresforschung, Bremerhaven, Germany

Abstract The amount of snow on Arctic sea ice impacts the ice mass budget. Wind redistribution of snow into open water in leads is hypothesized to cause significant wintertime snow loss. However, there are no direct measurements of snow loss into Arctic leads. We measured the snow lost in four leads in the Central Arctic in winter 2020. We find, contrary to expectations, that under typical winter conditions, minimal snow was lost into leads. However, during a cyclone that delivered warm air temperatures, high winds, and snowfall, 35.0 ± 1.1 cm snow water equivalent (SWE) was lost into a lead (per unit lead area). This corresponded to a removal of 0.7–1.1 cm SWE from the entire surface— $\sim 6\%$ – 10% of this site's annual snow precipitation. Warm air temperatures, which increase the length of time that wintertime leads remain unfrozen, may be an underappreciated factor in snow loss into leads.

Plain Language Summary The amount of snow on Arctic sea ice impacts how quickly the ice grows in the winter and melts in the summer. Cracks in the ice, known as leads, expose ocean water that snow can be blown into, reducing the amount of snow on the ice and thus impacting ice growth and melt. We found that in typical wintertime conditions, very little snow is blown into leads. However, if there is fresh snowfall, it is uncommonly warm and it is very windy at the same time when leads are forming, a large amount of snow can be blown into the ocean. Accounting for the impacts of air temperature on this process will enable scientists to better understand how much snow is on Arctic sea ice, and hence how quickly the ice grows in the winter and melts in the summer, and how this might change in a future, warmer, Arctic.

1. Introduction

Snow on Arctic sea ice impacts the energy budget and mass balance of the ice. The insulating properties of snow limit ice growth in the winter (Maykut & Untersteiner, 1971; Sturm et al., 2002) whereas its high albedo (Warren, 2019) slows ice melt in the summer (Perovich et al., 2002). Snow is a freshwater source for melt ponds (Polashenski et al., 2012) and habitat for biota (Iacozza & Ferguson, 2014). Despite this importance, the snow mass balance on Arctic sea ice remains uncertain. Several poorly-constrained processes contribute to the net budget, including: precipitation, deposition, sublimation, melting, flooding (snow-ice formation), superimposed ice formation, and wind-blown snow redistribution into open water leads (snow loss into leads).

Snow loss into leads has been estimated to consume up to 50% of the snowfall on Antarctic sea ice (Leonard & Maksym, 2011). The applicability of these estimates to the Arctic is unclear. There are no published direct measurements of snow loss into leads in the Arctic. Nevertheless, parameterizations of the process have been developed and implemented in climate models (Lecomte et al., 2015) and data assimilation products (Petty

© 2023. The Authors.

This is an open access article under the terms of the [Creative Commons Attribution License](https://creativecommons.org/licenses/by/4.0/), which permits use, distribution and reproduction in any medium, provided the original work is properly cited.

et al., 2018). For example, Petty et al. (2018) modeled that blowing snow loss into leads reduced the snow depth on sea ice North of 60°N by 10 cm throughout the winter (~25% reduction).

We present the first measurements of snow loss into Arctic leads from four cases we observed in detail in winter 2020 in the Atlantic sector of the Central Arctic Ocean. Snow loss into leads was determined from the $\delta^{18}\text{O}$ of the lead ice, a signature routinely used to identify snow contributions to sea ice (Arndt et al., 2021; Granskog et al., 2003, 2004, 2017; Jeffries et al., 1994, 1997, 2001; Kawamura et al., 2001; Tian et al., 2020). When snow enters seawater in a lead, the snow is less dense than seawater and consequently floats at the surface. If there is sufficient heat at the ocean surface to melt the snow, the resulting freshwater is less dense than seawater. As the lead freezes, the snow (solid or melted) is incorporated into the lead ice. Due to isotopic fractionation, snow is depleted in ^{18}O relative to seawater (Dansgaard, 1953). We contextualize the observations with atmospheric conditions at the time of lead formation to infer controls on snow loss into leads.

2. Materials and Methods

2.1. Overview of Data Collection

During the Multidisciplinary drifting Observatory for the Study of Arctic Climate (MOSAiC) expedition, R/V Polarstern drifted with an ice floe in the Arctic Ocean from October 2019 to May 2020 (Nicolaus et al., 2022; Rabe et al., 2022; Shupe et al., 2022). In March and April 2020, within 1 km of Polarstern, we observed the formation of ~18 leads ranging in width from 5 m to greater than 100 m. Whenever possible, we identified the timing of lead formation and refreezing to within 20 min by visual observations and time-lapse panoramic imagery (Nicolaus et al., 2021). Near-surface meteorology and localized snow depth were measured continuously from a tower and two mobile stations in the area nearby these active leads. Also observed continuously from the tower were mass fluxes of drifting and blowing snow at an average height of 0.1 m using a snow particle counter, which detected the number and sizes of horizontally-transported snow particles (SPC-95, Niigata Electric Co., Ltd.; M. M. Frey et al., 2020; Sato et al., 1993). Following Wagner et al. (2022) we assume that the snow particles are spherical with a density of 917 kg m^{-3} . Surface snow samples from various locations were collected approximately every other day and stable water isotopes were subsequently measured.

We studied the snow loss in four of the leads (described in Section 2.2) that formed in a range of conditions. From each lead, we collected 7–14 ice cores (9 cm diameter). Cores were drilled along transects perpendicular to (i.e., across) and parallel to (i.e., along) the leads with a spacing of 1–2.5 m between cores. Supporting Information S1 includes additional details on sampling (Text S1 in Supporting Information S1) and maps of lead locations (Figure S1 in Supporting Information S1). One or two cores from each lead were vertically sectioned into 5 cm samples in the field and the remainder were whole core samples. We recorded ice thickness, snow depth, freeboard, core length, and visual stratigraphy (locations and thicknesses of granular ice layers) in the field. Onboard Polarstern, we melted each sample and mixed it before measuring salinity (practical salinity scale) with a YSI Model 30 (<https://www.ysi.com/File%20Library/Documents/Manuals%20for%20Discontinued%20Products/030136-YSI-Model-30-Operations-Manual-RevE.pdf>) and completely filling and sealing a 20 mL subsample in a High-Density-Polyethylene vial. The $\delta^{18}\text{O}$ of the subsamples were determined in the central laboratory of the Swiss Federal Institute for Forest, Snow and Landscape, Birmensdorf, Switzerland with an Isotopic Water Analyzer IWA-45-ER (ABB - Los Gatos Research Inc., US). Measurement uncertainty for $\delta^{18}\text{O}$ was $\pm 1\text{‰}$, the precision $\pm 0.5\text{‰}$. Samples were measured in duplicate and averaged. The quality control was conducted with three standards for $\delta^{18}\text{O}$ at 0.00‰, -12.34‰ , and -55.50‰ are presented as per mil difference relative to VSMOW (‰, Vienna Standard Mean Ocean Water).

2.2. Lead Descriptions

Information on the four leads is presented in Table 1, Sections 2.2.1–2.2.4, and in Supporting Information S1.

2.2.1. SL Lead

The SL lead opened for the first time on 11 March and experienced numerous subsequent cycles of opening and refreezing followed by ridging and rafting. The ice we sampled formed in lead opening events on either 25–26 or 29–30 March. Although the date of ice formation is not known, the surface meteorology was similar during the two opening periods, with air temperatures close to climatological values (Rinke et al., 2021). We have combined

Table 1
Lead Characteristics

Lead	Date opened	Air temperature range ^a (°C)	Wind speed range ^a (m s ⁻¹)	Relative wind direction inter-quartile ^{a,b} (°)	Mean blowing snow flux ^a (kg m ⁻² s ⁻¹)	Date sampled	Width ^c (m)	Rafted ^c	Transect type(s)	Core spacing (m)	# of cores	# of sectioned cores
SL ^d	25 March	[-28.8, -24.1]	[6.5, 10.8]	[21, 32]	0.000357	15 April	40	Yes	Perpendicular and parallel	1	12	1
SL ^d	29 March	[-29.7, -24.2]	[3.0, 8.3]	[348, 357]	0.000498	15 April	40	Yes	Perpendicular and parallel	1	12	1
T	4 April	[-26.7, -21.3]	[3.3, 10.0]	[43, 73]	0.000008	15 April	8	Yes	Perpendicular and parallel	1	8	2
M	23 March	[-29.8, -25.5]	[0.6, 2.9]	[101, 145]	0.000000	18 April	23	No	Perpendicular and parallel	1–2.5	14	1
A	19 April	[-15.3, 0.0]	[0.6, 15.7]	[11, 214]	0.068550	24 & 28 April	6	No	Perpendicular	1	7	2

^aWhen the lead was open. ^bRelative wind direction follows the meteorological convention (direction wind is coming from, angles increasing clockwise) and has been rotated so a wind directly perpendicular to the lead is 0° or 180°, and directly parallel to the lead is 90° or 270°. ^cWhen the lead was sampled. ^dThere were two possible dates when the ice sampled in SL lead could have formed as described in Section 2.2.1.

these time periods in subsequent analysis (e.g., Figure 2a). Most ice cores contained a granular layer 3 cm thick at 15 cm depth (Figure 1a). This layer, combined with observations that the lead contracted after opening, indicated that the ice rafted after formation.

2.2.2. M Lead

The M lead opened around 4:00 UTC on 23 March. Within a few hours of opening, the lead was covered by a thin layer of nilas. Between 29 March and 1 April, a closing event reduced the lead's width by approximately half to 8 m wide. Afterward the lead remained quiescent. Most cores contained a granular layer 1 cm thick at 32 cm depth (Figure 1b), indicating that the ice rafted after formation.

2.2.3. T Lead

The T lead opened around 0:00 UTC 4 April. During 5–8 April, ice dynamics occurred in the center of the T lead but not where we would subsequently collect samples from. The T lead was split in the middle by a crack running parallel to the lead that opened the morning we sampled. Unfortunately, we were unable to access the ice on the upwind (at the time of lead formation) half of the lead on 15 April and this ice ridged in the following days.

2.2.4. A Lead

The A lead opened around 8:20 UTC 19 April during a warm air advection event associated with extreme warmth (Rinke et al., 2021), precipitation, and high winds originating from a cyclone moving northward from the Greenland Sea. During 19–20 April, the open water we observed in leads was not rapidly freezing. We visually estimated that the open water fraction in the area within 1 km of Polarstern was approximately 0.03. Within a 50 km radius of Polarstern, ice drift derived from subsequent SAR scenes indicates that divergent ice motion opened new leads covering approximately 0.02 of the area (these measurements do not preclude the persistence of open water from prior days).

Retrievals of precipitation based on a 35-GHz vertically-pointing radar mounted on the Polarstern deck indicate 1.04 cm of liquid-equivalent snowfall from 16 to 22 April (Matrosov et al., 2022). Blowing snow picked up around 0530 UTC on 20 April. The three stations on level ice near Polarstern with downward-pointing acoustic rangefinders observed accumulation generally coinciding with pulses of precipitation (documented by radar reflectivities), followed shortly by ablation. No net change in the surface height after the storm was observed, implying winds eroded all of the new, but none of the pre-existing snow. Repeat snow depth transects within 1 km of Polarstern at this time also did not record notable snow accumulation (Itkin et al., 2023). This suggests that much of the blowing snow during the A lead event was from concurrent precipitation.

Cores from the A lead on 24 April (Figure 1d) generally comprised about 27 cm of very soft ice overlying 31–37 cm of slush. Ice thickness measurements indicated that there were 10–20 cm of slush below this that the corer was unable to collect. The ice had a distinctive layer-cake-like structure with alternating light and dark 1–3 cm thick layers. We revisited the A lead on 28 April and collected a single core. This core was considerably more solid than those collected 4 days prior, but was otherwise similar.

2.3. Analysis of Snow Mass in Leads

Following Jeffries et al. (1994), Granskog et al. (2017), Tian et al. (2020), the $\delta^{18}\text{O}$ in a sample of sea ice is a mixture, by mass, of the $\delta^{18}\text{O}$ of pure snow—which we denote $\delta_{s,l}$ for lead l —and the $\delta^{18}\text{O}$ of snow-free sea ice—which we denote δ_{ref} (same notation as Granskog et al., 2017). Additionally, we represent the measurement uncertainty of the $\delta^{18}\text{O}$ measurement (Section 2.1) as Gaussian, uncorrelated noise—which we denote $\epsilon_{l,i}$ for sample i from lead l —with a standard deviation: $\sigma_\delta = 0.5 \text{ ‰}$. Equations 1 and 2 represent this model:

$$\delta_{l,i} = \frac{S_{l,i}}{t_{l,i}} \delta_{s,l} + \left(1 - \frac{S_{l,i}}{t_{l,i}}\right) \delta_{ref} + \epsilon_{l,i} \quad (1)$$

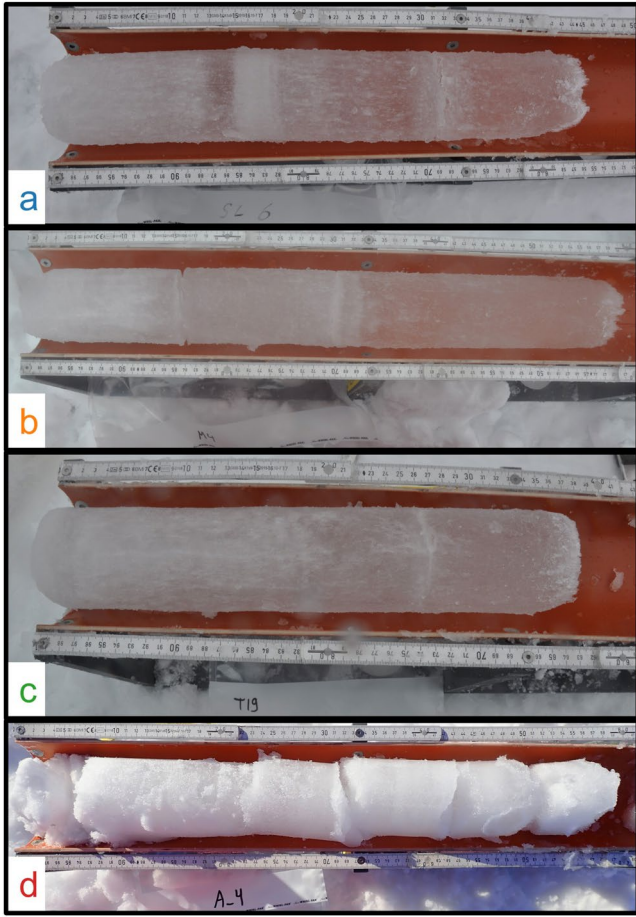


Figure 1. Representative ice cores from leads SL (a), M (b), T (c), and A (d). The top of each core is to the left. The SL and M cores contain granular layers around 15 and 30 cm respectively. The T core contains no granular layers below the top (the feature at 28 cm is a crack), and the A core is entirely opaque.

for the core from the sections. The likelihood ($\mathbb{P}(\delta_{l,i} | s_{l,i})$; Equations 4–6) follows from the mixture model (Equations 1 and 2). We have no prior information about the snow mass in these leads except that it is non-negative and cannot exceed the total mass of the ice ($t_{l,i}$). Thus we represent our prior ($\mathbb{P}(s_{l,i})$; Equation 7) as a uniform distribution on this domain. We numerically estimate $\mathbb{P}(s_{l,i} | \delta_{l,i})$ through grid sampling (Gelman et al., 2021, Chapter 10.3). The probability density of the mean SWE in each lead given the N samples from that lead ($\mathbb{P}(s_l | \delta_{l,1}, \delta_{l,2}, \dots, \delta_{l,N})$; Equation 8) is the conflation (Hill, 2011) of the sample probability densities ($\mathbb{P}(s_{l,i} | \delta_{l,i})$).

$$\mathbb{P}(s_{l,i} | \delta_{l,i}) \propto \mathbb{P}(\delta_{l,i} | s_{l,i}) \mathbb{P}(s_{l,i}) \quad (3)$$

$$\mathbb{P}(\delta_{l,i} | s_{l,i}) = \frac{1}{\sigma_{l,i} \sqrt{2\pi}} \exp\left(\frac{-(\delta_{l,i} - \mu_{l,i})^2}{2\sigma_{l,i}^2}\right) \quad (4)$$

$$\mu_{l,i} = \frac{s_{l,i}}{t_{l,i}} \mu_{s,l} + \left(1 - \frac{s_{l,i}}{t_{l,i}}\right) \mu_{ref} \quad (5)$$

$$\sigma_{l,i}^2 = \left(\frac{s_{l,i}}{t_{l,i}}\right)^2 \tau_{s,l}^2 + \left(1 - \frac{s_{l,i}}{t_{l,i}}\right)^2 \tau_{ref}^2 + \sigma_\delta^2 \quad (6)$$

$$\mathbb{P}(s_{l,i}) = U(0, t_{l,i}) \quad (7)$$

$$\epsilon_{l,i} \sim N(0, \sigma_\delta^2) \quad (2)$$

where $s_{l,i}$ is the snow water equivalent (SWE) in the sample and $t_{l,i}$ is the total water equivalent of the sample. $\frac{s_{l,i}}{t_{l,i}}$ is the mass fraction of snow in the ice.

The $\delta^{18}\text{O}$ of snow-free ice (δ_{ref}) is higher than that of pure sea water because fractionation during the freezing process enriches it in ^{18}O (K. Moore et al., 2017; Tian et al., 2020). We follow Granskog et al. (2017) and use the bottom ice samples of the sectioned cores (defined as ice below the lowest granular ice) to determine δ_{ref} . To account for the measurement uncertainty, we represent δ_{ref} as a normal distribution whose mean (μ_{ref}) and standard deviation (τ_{ref}) are estimated from the bottom ice samples via Bayesian inference with a noninformative prior (Gelman et al., 2021, Chapter 2.5).

The $\delta^{18}\text{O}$ of snow ($\delta_{s,l}$) varies depending on the provenance of the snow. In particular, snow precipitated from warmer air masses (e.g., the 16–21 April warm air intrusions) is less depleted in ^{18}O (has less negative $\delta^{18}\text{O}$) than snow from colder air masses. For the A lead event, we identified two surface snow samples that accumulated contemporaneously with snow blowing into A lead. We represent $\delta_{s,A}$ as a normal distribution whose mean ($\mu_{s,A}$) and standard deviation ($\tau_{s,A}$) are estimated from these surface snow samples in the same manner as δ_{ref} .

For the snow blown into the SL, M, and T leads, we could not unambiguously identify surface snow samples that accumulated during each event. The blowing snow during these events was likely re-mobilized snow. Eleven surface snow samples were collected from a week before the first lead opened to a week after the last lead refroze (16 March–12 April). To account for the fact that we do not know the precise provenance of the snow blown into these leads, we estimated the mean ($\mu_{s,(SL,M,T)}$) and standard deviation ($\tau_{s,(SL,M,T)}$) of $\delta_{s,(SL,M,T)}$ as the sample mean and standard deviation of these 11 samples. In this case, the uncertainty of the provenance greatly exceeds the measurement uncertainty.

We apply Bayes rule (Bayes & Price, 1763) to estimate the probability density of SWE in each core given its $\delta^{18}\text{O}$ measurement ($\mathbb{P}(s_{l,i} | \delta_{l,i})$; Equation 3). For sectioned cores, we computed the weighted-average (by section length) $\delta^{18}\text{O}$

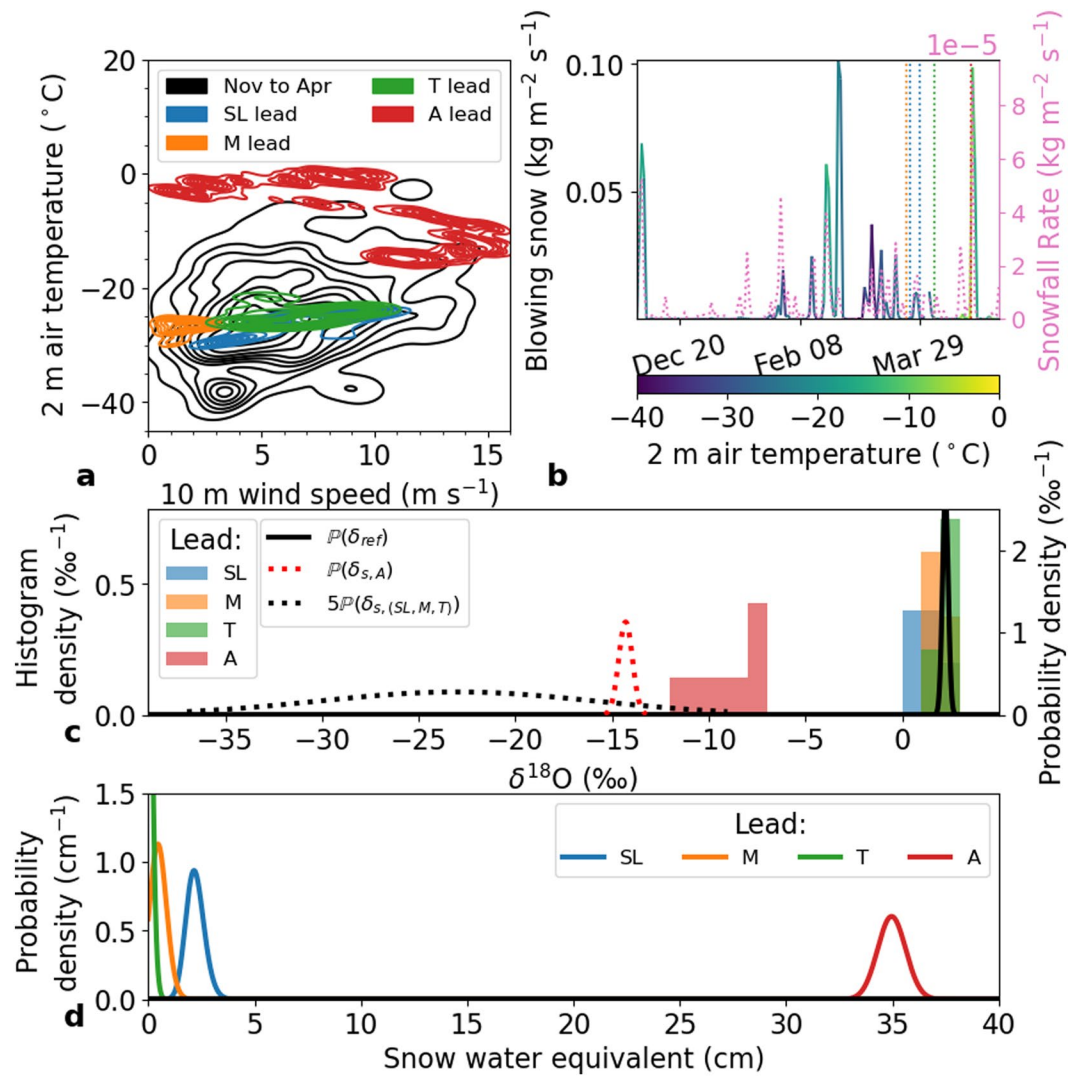


Figure 2. (a) The distribution of 10 m wind speed and 2 m air temperature for November to April at MOSAiC (black contours) with the distributions at the time of formation for each lead (colored contours). Contours indicate 10% density isolines. (b) Daily mean snow mass flux measured nominally 10 cm above the surface, colored by air temperature and snowfall rate (Matrosov et al., 2022). Formation dates of leads are indicated by vertical dotted lines (same colors as a, c, d). Both possible formation dates for ice in SL are indicated. (c) Histograms δ¹⁸O measurements for each lead (left axis) and distributions of δ¹⁸O for snow and snow-free ice (right axis). (d) Probability distributions of mean snow water equivalent in each lead.

$$\mathbb{P}(s_l | \delta_{l,1}, \delta_{l,2}, \dots, \delta_{l,N}) \propto \prod_{i=1}^N \mathbb{P}(s_{l,i} | \delta_{l,i}) \quad (8)$$

3. Results

During the A lead event, peak air temperatures reached ~0°C (16°C warmer than the November to April average) and it coincided with one of the largest blowing snow events (97th percentile) of December through April (Figures 2a and 2b). In contrast, the SL and T leads formed during typical temperature, wind, and blowing snow conditions (blowing snow at 66th and 33rd percentiles respectively; Figures 2a and 2b). During the formation of the M lead wind speeds were calmer than usual, temperatures were typical, and the blowing snow was at the ninth percentile.

The mean δ¹⁸O of the A lead (-8.9 ‰) was considerably lower than that of the SL, M, and T leads (1.2, 2.0, and 2.4 ‰ respectively). The δ¹⁸O of snow-free ice (δ_{ref}) was 2.24 ± 0.30 ‰ (all plus-minus at the 95% confidence

level; solid black line in Figure 2c). For the A lead event δ_{sA} was $-14.3 \pm 0.70 \text{ ‰}$ (dotted red line in Figure 2c). For the other leads δ_{sSLMT} was $-23.0 \pm 14.3 \text{ ‰}$ (dotted black line in Figure 2c). See Supporting Information S1 (Text S2 and Tables S1 and S2) for more information on $\delta^{18}\text{O}$ of snow and snow-free ice.

The SWE in the A lead ($35.0 \pm 1.1 \text{ cm}$; Figure 2d) was approximately 16 times greater per unit area than that in the SL lead ($2.2 \pm 0.7 \text{ cm}$)—the next highest. The M lead contained just 0.6 cm of SWE (95% credible interval 0.1–1.2 cm). Given the low winds and minimal blowing snow, much of this must have been interred by rafting. Finally, we found minimal—if any—SWE in the T lead (95% credible interval 0.0–0.4 cm). The mean snow percentages, by mass, in the A, SL, M, and T leads were 67.5%, 3.8%, 1.1%, and 0.3% respectively.

The open water fraction during the A lead event was approximately 0.03 within 1 km of Polarstern and 0.02 within 50 km of Polarstern (Section 2.2.4). Thus, if the snow loss into A lead were typical of the event, snow loss may have reduced the snow budget by approximately 0.7–1.1 cm SWE. The other three lead events had a negligible impact on the snow budget.

4. Discussion

4.1. Minimal Snow Loss in Typical Wintertime Conditions

Our results suggest that in typical wintertime conditions at MOSAiC (characterized by the SL and T leads), minimal snow was lost into open water leads in the Arctic pack ice. First, at MOSAiC major blowing snow events—like the A lead event—were responsible for most of the blowing snow flux near the surface, but they occurred rarely and appear limited by the frequency of precipitation events. The 10 days (6.6% of the data) with the highest blowing snow flux at MOSAiC accounted for 70% of the total cumulative blowing snow flux. All but one of these days came during or immediately after the five major snowfall events on MOSAiC (Wagner et al., 2022). Little snow is likely to be deposited in leads outside of a major blowing snow event. Second, at typical wintertime air temperatures, open water in leads rapidly refreezes—limiting snow loss. We discuss this process in more detail in Section 4.3. From November through April, only 4.3% of days had mean air temperatures above -10°C : two days in mid-November and six days in April (including the A lead event). Unfortunately, neither blowing snow flux data nor $\delta^{18}\text{O}$ lead ice samples are available for the mid-November event, so we cannot assess the amount of snow loss into leads. But it was potentially a high snow loss into leads event due to high wind speeds (mean 10.6 m s^{-1} on November 16) and observations of open water around the Polarstern. Besides the A lead and possibly mid-November events, the impact of snow loss into leads on the snow mass budget at MOSAiC was likely minor. von Albedyll et al. (2022) estimated that from 14 October to 17 April, ice growth in leads contributed 0.1 m to the mean ice thickness. The mean snow percentages in our typical leads ranged from 0.3% (T lead) to 3.8% (SL lead). If these snow percentages were characteristic of ice grown in leads, then snow loss into typical wintertime leads consumed 0.02–0.34 cm SWE or approximately 0.2%–3.2% of the total annual snow precipitation (Wagner et al., 2022).

4.2. Significant Snow Loss in Exceptional Conditions

If there is a recent snowfall, high winds, and open water remains unfrozen (due to high temperatures), a significant amount of snow can be lost into leads, even at open water fractions under 0.05. At MOSAiC, approximately 1.04 cm SWE precipitated immediately before and during the A lead event and 9.8–11.4 cm SWE precipitated at MOSAiC throughout the accumulation season (Matrosov et al., 2022; Wagner et al., 2022). Thus, snow loss into open water during the A lead event may have consumed 65%–100% of the recent precipitation and 6%–10% of the total annual snow precipitation. This is consistent with the observation that no net accumulation occurred at the three meteorological stations (Section 2.2.4). Additionally, large snow loss during the A lead event is consistent with estimates during a warm storm event in the Bellinghousen Sea that all recent precipitation was lost into leads (Leonard & Maksym, 2011).

The A lead event was associated with a cyclone and warm air intrusion that advected warm air from the Atlantic and produced record-breaking warm and moist atmospheric conditions at the MOSAiC site (Rinke et al., 2021). While the April 2020 event was extreme, warming events are possibly becoming more common (G. W. K. Moore, 2016). The frequency of winter warming events North of 85°N roughly doubled from 1980 to 2015 (Graham et al., 2017). Further research is needed to explore the connections between snow loss into leads,

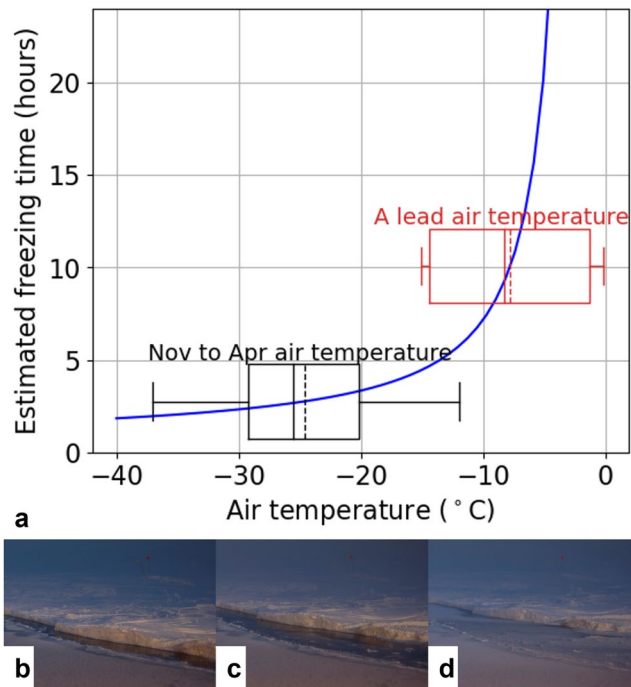


Figure 3. (a) Estimated time required to freeze 3 cm of ice thickness in a 20-m-wide lead at a wind speed of 6 m s^{-1} for a given air temperature, only accounting for turbulent heat flux (estimated from Andreas & Cash, 1999). Boxes show interquartile ranges and whiskers show 90% ranges of air temperatures at MOSAiC. (b–d) Images of a freezing lead at MOSAiC. In (b) the ice has just opened up, exposing open water between the mature ice and the young ice (closer to the camera) which had formed a few hours prior. Within 20 min, panel (c) shows that a thin skim of ice has frozen over the open water (the mature ice has also retreated exposing more open water). Within 2 hr, panel (d) shows that this new ice is sufficiently solid to accumulate snow on top of it.

into leads during major blowing snow events at a range of air temperatures are needed. One limitation of this work is that we do not have ice samples from leads that formed during cold major blowing snow events. This temperature dependence could also be considered in models that represent snow loss into leads (e.g., Hunke et al., 2017; Petty et al., 2018), and it is important that models accurately simulate freezing times. Additionally, the net impacts of snow loss into leads on the ice mass budget are uncertain. The immediate impact of snow in leads on the ice budget is positive (the snow turns into ice), but the net effect may depend on the timing of snow loss events. If there were less snow on Arctic sea ice, it would increase thermodynamic ice growth in the winter (Maykut & Untersteiner, 1971; Sturm et al., 2002) but reduce the albedo (Perovich & Elder, 2002; Perovich & Polashenski, 2012), which increases ice melt in the summer. Thus, autumn snow loss events may increase the ice mass budget whereas spring snow loss events likely decrease it. Further observations and modeling are needed to investigate these competing effects.

5. Conclusions

We presented the first direct observations of snow loss into leads in the Arctic from four leads at MOSAiC. Three leads formed under typical, cold winter conditions and contained $<2.9 \text{ cm SWE}$. Under typical winter conditions at MOSAiC, the impact of leads on the snow budget was likely minor. However, one lead contained $35.0 \pm 1.1 \text{ cm SWE}$ and was associated with a cyclone which delivered snowfall, high winds, and record-breaking warm temperatures. During this event, open water may have consumed 65%–100% of recent snow precipitation and approximately 6%–10% of annual snow precipitation. The frequency of such extreme events may be important for the snow budget on Arctic sea ice. Finally, this event highlighted that the duration of open water in leads,

cyclones, and warm air intrusions—and how these events might change snow loss in a changing climate.

4.3. Impacts of Temperature on the Duration of Open Water in Leads

Once the surface of a lead is frozen, snow cannot directly enter open water. Due to enhanced turbulent heat flux (Andreas & Cash, 1999), leads under colder air freeze faster (Figure 3a). For example, on 11 March at an air temperature of -25°C , we observed a thin ice skin form on a 1–2 m wide lead within 20 min. This lead was sufficiently refrozen to support snow on top of it within 2 hr (Figures 3b–3d). In contrast, the leads during the A lead event stayed unfrozen for 2 days, likely due to the near-freezing air temperature suppressing the turbulent heat flux. Accounting for only turbulent heat fluxes (Andreas & Cash, 1999), a hypothetical 20-m-wide lead under a wind speed of 6 m s^{-1} could freeze 3.6 times faster at an air temperature of -24.6°C (the November to April mean) than at a temperature of -7.8°C (the A lead event mean; Figure 3a). Given a constant snow flux, the cold lead would consume 72% less snow than the warm one. The exact values change slightly with our assumptions about lead width and wind speed, but the overall pattern is that the duration of open water in leads increases dramatically for air temperatures above approximately -10°C .

Accounting for the impacts of air temperature on the duration of open water in leads may be important for models and data assimilation products representing snow loss into leads. For example, some snow data assimilation products use passive microwave sea ice concentration products (e.g., Comiso, 1986) that misclassify thin ice as open water (Ivanova et al., 2015). Utilizing such products without accounting for the impacts of air temperature on the duration of open water could overestimate snow loss into leads.

4.4. Outlook

Further work is needed to quantify the relationship between air temperature and snow loss into open water. In particular, observations of snow loss

Acknowledgments

Data used in this manuscript were produced as part of the international MOSAiC project with the tag MOSAiC20192020 and the Project_ID: AWI_PS122_00. We thank all people involved in the expedition of the research vessel Polarstern (Knust, 2017) during MOSAiC in 2019–2020 as listed in Nixdorf et al. (2021). In particular, we thank Eric Brossier, Thomas Olufson, Delphin Ruché, and Saga Svavarsdóttir, for their capable assistance in the field. Thank you to Manuel Ernst for assistance with the time lapse imagery. DCS, CP, and DP were supported by NSF OPP-1724540. MMF was supported by the UK Natural Environment Research Council (NERC) (NE/S00257X/1), the NERC National Capability International grant SURFACE FluxEs In AnTArctica (SURFEIT) (NE/X009319/1), and the European Union's Horizon 2020 research and innovation programme under grant agreement No 101003826 via project CRiceS (Climate Relevant interactions and feedbacks: the key role of sea ice and Snow in the polar and global climate system). MAG was supported by the Norwegian Polar Institute and funding from the Research Council of Norway for project HAVOC (Grant 280292). JS received funding from the Swiss National Science Foundation (Grant 188478) and the Swiss Polar Institute. JS holds the Ingvar Kamprad Chair for Extreme Environments Research sponsored by Ferring Pharmaceuticals. JKH was supported by NSF OPP-1722729. L.vA was funded by the Alfred-Wegener-Institut, Helmholtz-Zentrum für Polar- und Meeresforschung through the project AWI_ICE. SWF was supported by the National Aeronautics and Space Administration Cryospheric Sciences Internal Scientist Funding Model (ISFM). ARM was supported by the WSL Institute for Snow and Avalanche Research SLF. WSL_201812N1678. Funder ID: <http://dx.doi.org/10.13039/501100015742>, the Swiss Polar Institute (SPI reference DIRCR-2018-003) Funder ID <http://dx.doi.org/10.13039/501100015594> and the European Union's Horizon 2020 research and innovation program projects ARICE (Grant 730965) for berth fees associated with the participation of the DEARice project. SA was supported by the German Research Council (DFG) in the framework of the priority program "Antarctic Research with comparative investigations in the Arctic ice areas" (Grants SPP1158 and AR1236/1) and by the Alfred-Wegener-Institut, Helmholtz-Zentrum für Polar- und Meeresforschung. CJC and meteorological data were supported by the NOAA Physical Sciences Laboratory (PSL), NOAA's Global Ocean Monitoring and Observing program (GOMO) (FundRef <https://doi.org/10.13039/100018302>), and the National Science Foundation (Grant

which increases dramatically with warmer air temperature, may be an underappreciated factor in how much snow can be lost into leads.

Data Availability Statement

Data from lead cores is available at Clemens-Sewall et al. (2022). Surface meteorology data are available at Cox, Gallagher, Shupe, Persson, Blomquist, et al. (2023), Cox, Gallagher, Shupe, Persson, Grachev, et al. (2023a, 2023b). Snow surface isotope data are available at Macfarlane et al. (2022). Blowing snow flux data are available at M. Frey et al. (2023).

References

Andreas, E. L., & Cash, B. A. (1999). Convective heat transfer over wintertime leads and polynyas. *Journal of Geophysical Research*, *104*(C11), 25721–25734. <https://doi.org/10.1029/1999JC900241>

Arndt, S., Haas, C., Meyer, H., Peeken, I., & Krumpen, T. (2021). Recent observations of superimposed ice and snow ice on sea ice in the north-western Weddell Sea. *The Cryosphere*, *15*(9), 4165–4178. <https://doi.org/10.5194/tc-15-4165-2021>

Bayes, T., & Price, N. (1763). LII. An essay towards solving a problem in the doctrine of chances. By the late Rev. Mr. Bayes, F. R. S. communicated by Mr. Price, in a letter to John Canton, A. M. F. R. S. *Philosophical Transactions of the Royal Society of London*, *53*, 370–418. <https://doi.org/10.1098/rstl.1763.0053>

Clemens-Sewall, D., Macfarlane, A., Fons, S., Granskog, M., Hutchings, J., & Schmale, J. (2022). *Salinity and stable water isotopes for ice cores in leads during leg 3 of the multidisciplinary drifting observatory for the study of Arctic climate 2020*. Arctic Data Center. Arctic Data Center. <https://doi.org/10.18739/A23N20G15>

Comiso, J. C. (1986). Characteristics of Arctic Winter Sea ice from satellite multispectral microwave observations. *Journal of Geophysical Research*, *91*(C1), 975–994. <https://doi.org/10.1029/JC091iC01p00975>

Cox, C., Gallagher, M., Shupe, M., Persson, O., Blomquist, B., Grachev, A., et al. (2023). *Met City meteorological and surface flux measurements (Level 2 Processed), Multidisciplinary drifting observatory for the study of arctic climate (MOSAIC), central Arctic, October 2019 - September 2020*. Arctic Data Center. Arctic Data Center. <https://doi.org/10.18739/A2TM7227K>

Cox, C., Gallagher, M., Shupe, M., Persson, O., Grachev, A., Solomon, A., et al. (2023a). *Atmospheric surface flux station #30 measurements (Level 2 Processed), multidisciplinary drifting observatory for the study of arctic climate (MOSAIC), central Arctic, October 2019 - September 2020*. Arctic Data Center. Arctic Data Center. <https://doi.org/10.18739/A2K649V1F>

Cox, C., Gallagher, M., Shupe, M., Persson, O., Grachev, A., Solomon, A., et al. (2023b). *Atmospheric surface flux Station #50 measurements (Level 2 Complete), multidisciplinary drifting observatory for the study of arctic climate (MOSAIC), central Arctic, October 2019 - September 2020*. Arctic Data Center. Arctic Data Center. <https://doi.org/10.18739/A2251FM5R>

Dansgaard, W. (1953). The Abundance of O¹⁸ in atmospheric water and water vapour. *Tellus*, *5*(4), 461–469. <https://doi.org/10.1111/j.2153-3490.1953.tb01076.x>

Frey, M., Wagner, D., Kirchgassner, A., Uttal, T., & Shupe, M. (2023). Atmospheric snow particle flux in the central Arctic during MOSAiC 2019–20. NERC EDS UK polar data Centre. Artwork Size: 424 files, 131 MB Pages: 424 files, 131 MB. <https://doi.org/10.5285/7D8E401B-2C75-4EE4-A753-C24B7E91E6E9>

Frey, M. M., Norris, S. J., Brooks, I. M., Anderson, P. S., Nishimura, K., Yang, X., et al. (2020). First direct observation of sea salt aerosol production from blowing snow above sea ice. *Atmospheric Chemistry and Physics*, *20*(4), 2549–2578. <https://doi.org/10.5194/acp-20-2549-2020>

Gelman, A., Carlin, J. B., Stern, H. S., Dunson, D. B., Vehtari, A., & Rubin, D. B. (2021). *Bayesian data analysis* Third edition (with errors fixed as of 15 February 2021) (3rd ed.). Columbia University Department of Statistics. Retrieved from <http://www.stat.columbia.edu/~gelman/book/>

Graham, R. M., Cohen, L., Petty, A. A., Boisvert, L. N., Rinke, A., Hudson, S. R., et al. (2017). Increasing frequency and duration of Arctic winter warming events. *Geophysical Research Letters*, *44*(13), 6974–6983. <https://doi.org/10.1002/2017GL073395>

Granskog, M. A., Leppäranta, M., Kawamura, T., Ehn, J., & Shirasawa, K. (2004). Seasonal development of the properties and composition of land-fast sea ice in the Gulf of Finland, the Baltic Sea. *Journal of Geophysical Research*, *109*(C2), C02020. <https://doi.org/10.1029/2003JC001874>

Granskog, M. A., Martma, T. A., & Vaikmäe, R. A. (2003). Development, structure and composition of land-fast sea ice in the northern Baltic Sea. *Journal of Glaciology*, *49*(164), 139–148. <https://doi.org/10.3189/172756503781830872>

Granskog, M. A., Rösel, A., Dodd, P. A., Divine, D., Gerland, S., Martma, T., & Leng, M. J. (2017). Snow contribution to first-year and second-year Arctic sea ice mass balance north of Svalbard. *Journal of Geophysical Research: Oceans*, *122*(3), 2539–2549. <https://doi.org/10.1002/2016JC012398>

Hill, T. (2011). Conflations of probability distributions. *Transactions of the American Mathematical Society*, *363*(6), 3351–3372. <https://doi.org/10.1090/S0002-9947-2011-05340-7>

Hunke, E., Lipscomb, W., Jones, P., Turner, A., Jeffery, N., & Elliott, S. (2017). CICE, the Los Alamos Sea Ice model (Tech. Rep. No. CICE; 005315WKSTN00). Los Alamos National Lab. (LANL). Retrieved from <https://www.osti.gov/biblio/1364126>

Iacozza, J., & Ferguson, S. H. (2014). Spatio-temporal variability of snow over sea ice in western Hudson Bay, with reference to ringed seal pup survival. *Polar Biology*, *37*(6), 817–832. <https://doi.org/10.1007/s00300-014-1484-z>

Itkin, P., Hendricks, S., Webster, M., von Albedyll, L., Arndt, S., Divine, D., et al. (2023). Sea ice and snow characteristics from year-long transects at the MOSAiC Central Observatory. *Elementa: Science of the Anthropocene*, *11*(1), 00048. <https://doi.org/10.1525/elementa.2022.00048>

Ivanova, N., Pedersen, L. T., Tonboe, R. T., Kern, S., Heygster, G., Lavergne, T., et al. (2015). Inter-comparison and evaluation of sea ice algorithms: Towards further identification of challenges and optimal approach using passive microwave observations. *The Cryosphere*, *9*(5), 1797–1817. <https://doi.org/10.5194/tc-9-1797-2015>

Jeffries, M. O., Krouse, H. R., Hurst-Cushing, B., & Maksym, T. (2001). Snow-ice accretion and snow-cover depletion on Antarctic first-year sea-ice floes. *Annals of Glaciology*, *33*, 51–60. <https://doi.org/10.3189/172756401781818266>

Jeffries, M. O., Morris, K., Weeks, W. F., & Worby, A. P. (1997). Seasonal variations in the properties and structural composition of sea ice and snow cover in the Bellingshausen and Amundsen Seas, Antarctica. *Journal of Glaciology*, *43*(143), 138–151. <https://doi.org/10.3189/S0022143000002902>

Jeffries, M. O., Shaw, R. A., Morris, K., Veazey, A. L., & Krouse, H. R. (1994). Crystal structure, stable isotopes (δ¹⁸O), and development of sea ice in the Ross, Amundsen, and Bellingshausen seas, Antarctica. *Journal of Geophysical Research*, *99*(C1), 985–995. <https://doi.org/10.1029/93JC02057>

OPP-1724551). We thank editor Rajaram and the two anonymous reviewers whose suggestions improved the manuscript.

- Kawamura, T., Shirasawa, K., Ishikawa, N., Lindfors, A., Rasmus, K., Granskog, M. A., et al. (2001). Time-series observations of the structure and properties of brackish ice in the Gulf of Finland. *Annals of Glaciology*, 33, 1–4. <https://doi.org/10.3189/172756401781818950>
- Knust, R. (2017). Polar research and supply vessel POLARSTERN operated by the Alfred-Wegener-institute. *Journal of Large-Scale Research Facilities JLSRF*, 3(0), A119. <https://doi.org/10.17815/jlsrf-3-163>
- Lecomte, O., Fichefet, T., Flocco, D., Schroeder, D., & Vancoppenolle, M. (2015). Interactions between wind-blown snow redistribution and melt ponds in a coupled ocean-sea ice model. *Ocean Modelling*, 87, 67–80. <https://doi.org/10.1016/j.ocemod.2014.12.003>
- Leonard, K. C., & Maksym, T. (2011). The importance of wind-blown snow redistribution to snow accumulation on Bellingshausen Sea ice. *Annals of Glaciology*, 52(57), 271–278. <https://doi.org/10.3189/172756411795931651>
- Macfarlane, A. R., Schneebeli, M., Dacic, R., Wagner, D. N., Arndt, S., Clemens-Sewall, D., et al. (2022). Snowpit stable isotope profiles during the MOSAiC expedition [Dataset]. PANGAEA. <https://doi.org/10.1594/PANGAEA.952556>
- Matrosov, S. Y., Shupe, M. D., & Uttal, T. (2022). High temporal resolution estimates of Arctic snowfall rates emphasizing gauge and radar-based retrievals from the MOSAiC expedition. *Elementa: Science of the Anthropocene*, 10(1), 00101. <https://doi.org/10.1525/elementa.2021.00101>
- Maykut, G. A., & Untersteiner, N. (1971). Some results from a time-dependent thermodynamic model of sea ice. *Journal of Geophysical Research*, 76(6), 1550–1575. <https://doi.org/10.1029/JC076i006p01550>
- Moore, G. W. K. (2016). The December 2015 north pole warming event and the increasing occurrence of such events. *Scientific Reports*, 6(1), 39084. <https://doi.org/10.1038/srep39084>
- Moore, K., Fayek, M., Lemes, M., Rysgaard, S., & Holländer, H. M. (2017). Fractionation of hydrogen and oxygen in artificial sea ice with corrections for salinity for determining meteorological water content in bulk ice samples. *Cold Regions Science and Technology*, 142, 93–99. <https://doi.org/10.1016/j.coldregions.2017.07.011>
- Nicolaus, M., Arndt, S., Birnbaum, G., & Katlein, C. (2021). Visual panoramic photographs of the surface conditions during the MOSAiC campaign 2019/20. PANGAEA. <https://doi.org/10.1594/PANGAEA.938534>
- Nicolaus, M., Perovich, D. K., Spreen, G., Granskog, M. A., von Albedyll, L., Angelopoulos, M., et al. (2022). Overview of the MOSAiC expedition: Snow and sea ice. *Elementa: Science of the Anthropocene*, 10(1), 000046. <https://doi.org/10.1525/elementa.2021.000046>
- Nixdorf, U., Dethloff, K., Rex, M., Shupe, M., Sommerfeld, A., Perovich, D. K., et al. (2021). MOSAiC extended acknowledgement. Zenodo. <https://doi.org/10.5281/zenodo.5541624>
- Perovich, D. K., & Elder, B. (2002). Estimates of ocean heat flux at SHEBA. *Geophysical Research Letters*, 29(9), 58-1–58-4. <https://doi.org/10.1029/2001GL014171>
- Perovich, D. K., Grenfell, T. C., Light, B., & Hobbs, P. V. (2002). Seasonal evolution of the albedo of multiyear Arctic sea ice. *Journal of Geophysical Research*, 107(C10), SHE20-1–SHE20-13. <https://doi.org/10.1029/2000JC000438>
- Perovich, D. K., & Polashenski, C. (2012). Albedo evolution of seasonal Arctic sea ice. *Geophysical Research Letters*, 39(8), L08501. <https://doi.org/10.1029/2012GL051432>
- Petty, A. A., Webster, M., Boisvert, L., & Markus, T. (2018). The NASA Eulerian snow on Sea Ice model (NESOSIM) v1.0: Initial model development and analysis. *Geoscientific Model Development*, 11(11), 4577–4602. <https://doi.org/10.5194/gmd-11-4577-2018>
- Polashenski, C., Perovich, D., & Courville, Z. (2012). The mechanisms of sea ice melt pond formation and evolution. *Journal of Geophysical Research*, 117(C1). <https://doi.org/10.1029/2011JC007231>
- Rabe, B., Heuzé, C., Regnery, J., Aksenov, Y., Allerholt, J., Athanase, M., et al. (2022). Overview of the MOSAiC expedition: Physical oceanography. *Elementa: Science of the Anthropocene*, 10(1), 00062. <https://doi.org/10.1525/elementa.2021.00062>
- Rinke, A., Cassano, J. J., Cassano, E. N., Jaiser, R., & Handorf, D. (2021). Meteorological conditions during the MOSAiC expedition: Normal or anomalous? *Elementa: Science of the Anthropocene*, 9(1), 00023. <https://doi.org/10.1525/elementa.2021.00023>
- Sato, T., Kimura, T., Ishimaru, T., & Maruyama, T. (1993). Field test of a new snow-particle counter (SPC) system. *Annals of Glaciology*, 18, 149–154. <https://doi.org/10.3189/S0260305500011411>
- Shupe, M. D., Rex, M., Blomquist, B., Persson, P. O. G., Schmale, J., Uttal, T., et al. (2022). Overview of the MOSAiC expedition: Atmosphere. *Elementa: Science of the Anthropocene*, 10(1), 00060. <https://doi.org/10.1525/elementa.2021.00060>
- Sturm, M., Perovich, D. K., & Holmgren, J. (2002). Thermal conductivity and heat transfer through the snow on the ice of the Beaufort Sea. *Journal of Geophysical Research*, 107(C10), SHE19-1–SHE19-17. <https://doi.org/10.1029/2000JC000409>
- Tian, L., Gao, Y., Weisling, B., & Ackley, S. F. (2020). Snow-ice contribution to the structure of sea ice in the Amundsen Sea, Antarctica. *Annals of Glaciology*, 61(83), 369–378. <https://doi.org/10.1017/aog.2020.55>
- von Albedyll, L., Hendricks, S., Grodzifig, R., Krumpfen, T., Arndt, S., Belter, H. J., et al. (2022). Thermodynamic and dynamic contributions to seasonal Arctic sea ice thickness distributions from airborne observations. *Elementa: Science of the Anthropocene*, 10(1), 00074. <https://doi.org/10.1525/elementa.2021.00074>
- Wagner, D. N., Shupe, M. D., Cox, C., Persson, O. G., Uttal, T., Frey, M. M., et al. (2022). Snowfall and snow accumulation during the MOSAiC winter and spring seasons. *The Cryosphere*, 16(6), 2373–2402. <https://doi.org/10.5194/16-2373-2022>
- Warren, S. G. (2019). Optical properties of ice and snow. *Philosophical Transactions of the Royal Society A: Mathematical, Physical & Engineering Sciences*, 377(2146), 20180161. <https://doi.org/10.1098/rsta.2018.0161>

References From the Supporting Information

- Hutter, N., Hendricks, S., Jutila, A., Ricker, R., von Albedyll, L., Birnbaum, G., & Haas, C. (2021). Gridded airborne laserscanner (ALS) elevation data (L4) for three flights during MOSAiC (prerelease). Zenodo. <https://doi.org/10.5281/ZENODO.5121823>